Asymptotic Stability of an Eikonal Transformation Based ADI Method for the Paraxial Helmholtz Equation at High Wave Numbers

Qin Sheng[1,*], and Hai-Wei Sun[2]

[1] *Center for Astrophysics, Space Physics and Engineering Research, Department of Mathematics, Baylor University, Waco, TX 76798-7328, USA.*
[2] *Department of Mathematics, University of Macau, Macao, P.R. China*

Abstract. This paper concerns the numerical stability of an eikonal transformation based splitting method which is highly effective and efficient for the numerical solution of paraxial Helmholtz equation with a large wave number. Rigorous matrix analysis is conducted in investigations and the oscillation-free computational procedure is proven to be stable in an asymptotic sense. Simulated examples are given to illustrate the conclusion.

AMS subject classifications: 65M06, 65M12, 65F35, 15A12

Key words: paraxial equation, highly oscillatory problems, eikonal splitting, asymptotic stability, matrix eigenvalues, spectral radius.

1 Introduction

Fast and accurate analysis of optical wave devices such as waveguides and couplers have been crucial to the development of light integrated systems [4, 13]. Core parts of such analysis often involve advanced computational procedures for investigating the wave propagation characteristics of the particular system. While the beam propagation method, which is based on fast Fourier transforms, has been popular in the study [7,8,17], different finite difference schemes are also employed in the research. To improve the accuracy of a numerical method used, a traditional approach is to increase the density of the grid or decrease the mesh step sizes utilized [4, 8, 9]. With a uniform mesh and step size, the cost for doing so may quickly become prohibitive if a high wave frequency is encountered. Nonuniform mesh structures and step sizes, on the other hand, may offer certain advantages in the situation [9,15]. However, they are often cumbersome to implement in industrial applications [3, 13]. The issue of computational efficiency has become

*Corresponding author. *Email addresses:* qin_sheng@baylor.edu (Q. Sheng), HSun@umac.mo (H. Sun)

increasingly important in certain applications, in particular in the development of highly accurate, yet rapid numerical methods for solving paraxial, or parabolic, wave equations in order to separate inaccuracies inherent in numerical methods from inaccuracies due to paraxial wave approximations under modern laser configurations [12,13,16].

Consider a slowly varying envelope approximation of the light beam. A frequently used paraxial optical wave model is the Helmholtz equation,

$$2\mathbf{i}\kappa_0 l_0 E_z = E_{xx} + E_{yy} + \kappa_0^2 \left[l^2(x,y,z) - l_0^2 \right] E, \quad (x,y,z) \in \mathcal{D}, \tag{1.1}$$

where E is the electric field function of the light wave within a narrow cone, z is the beam propagation direction, x,y are transverse directions perpendicular to the light, $\mathbf{i} = \sqrt{-1}$, κ_0 is the wavenumber in free space, l_0 is the reference refractive index and $l(x,y,z)$ is the cross section index profile [4,7,9]. The differential equation provides solutions that describe the propagation of electromagnetic waves in the form of either paraboloidal waves or Gaussian beams. Most lasers emit beams that take the latter form [4,8]. The paraxial wave equation (1.1) can be viewed as a simplification of Maxwell's field equations [1,8,11,13]. Without loss of generality, we set $\mathcal{D} = \{a < x < b,\ c < y < d,\ z > z_0\}$.

Since the wave parameter $\kappa = \kappa_0 l_0$ is large in optical applications, the field function E is highly oscillatory. This may considerably impair our desire for a higher computational efficiency as well as accuracy in a traditional way, since mesh steps cannot be unrealistically small [6,14,18].

This motivates the latest search for eikonal transformation based numerical methods. The idea is straightforward. Let $\phi(x,y,z)$ and $\psi(x,y,z)$ be sufficiently smooth real functions satisfying conditions

$$|\phi_z| \ll \kappa|\phi|,\ |\phi_{zz}| \ll \kappa^2|\phi|, \quad (x,y,z) \in \mathcal{D}. \tag{1.2}$$

We then look for the solution of (1.1) in the form of

$$E(x,y,z) = \phi(x,y,z) e^{\mathbf{i}\kappa\psi(x,y,z)}, \quad (x,y,z) \in \mathcal{D}. \tag{1.3}$$

In fact, functions ϕ and ψ are closely related to the amplitude and ray, or eikonal, functions corresponding to the electric field E, respectively. The constraint (1.2) coincides with the basic feature of paraxial waves, that is,

$$\sin\theta \approx \theta,\ \tan\theta \approx \theta,$$

where θ is the angle between the beam vector and optical axis [1,8]. Transformations similar to (1.3) have also been used frequently in Wentzel-Kramers-Brillouin (WKB), or semiclassical, approximations in quantum physics.

The aim of this paper is not for a refinement of existing models, or a continue development of new schemes. Instead, we will focus at the numerical stability of the latest alternative direction implicit (ADI) method acquired. Our discussion will be comprised as follows. In the next section, a key feature of the eikonal transformation (1.3) will be

explored. From it, the detailed matrix structure of our transformation based ADI scheme will be derived. Section 3 will be devoted to investigations of the asymptotic stability of the eikonal splitting method via rigorous matrix spectrum analysis. Finally, in Section 4, computational experiments illustrating the numerical stability of the underlying algorithm will be presented. Concluding remarks will also be given.

2 Eikonal Transformation Based ADI Method

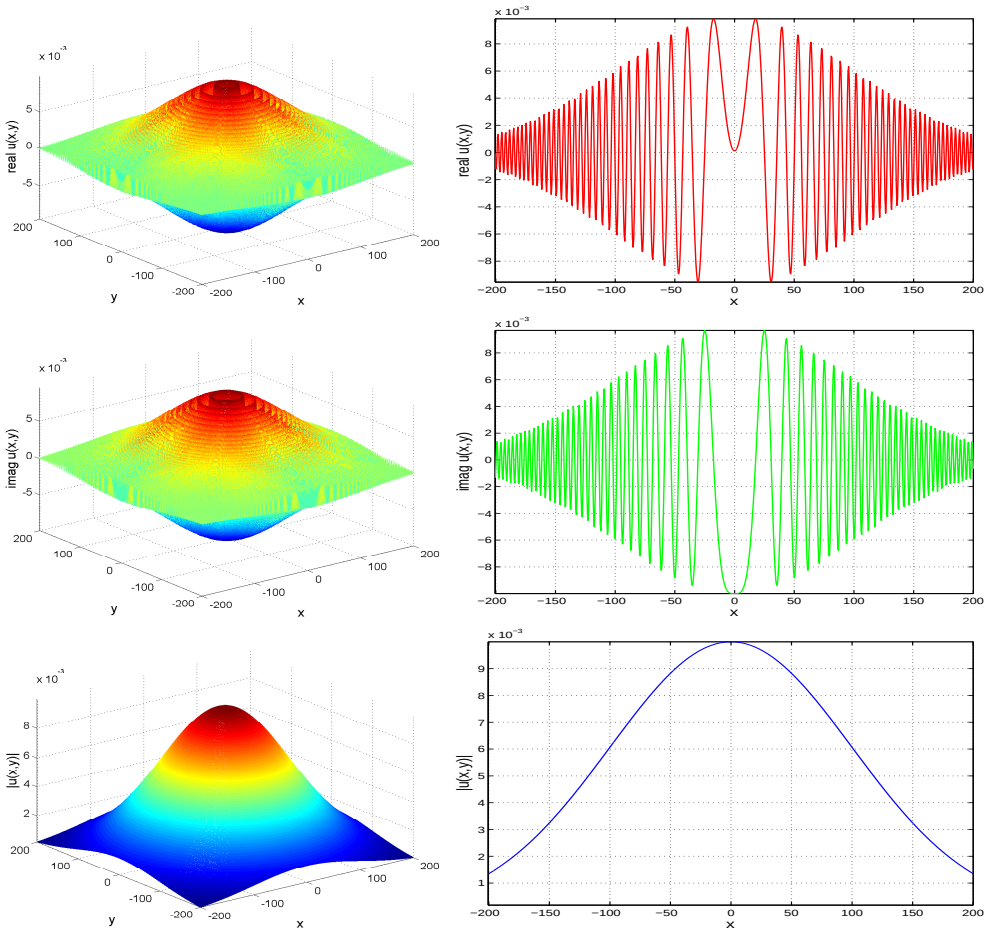

FIGURE 2.1. The real part, imaginary part, and modulus of the field function E given in (2.1). Spatial steps $h_x = h_y = 0.5$ are used. The second column is for intersections of the wave functions and the Y-Z plane. To view more details, the spacial domain is slightly reduced from its original size.

Consider a typical Gaussian beam solution of the Helmholtz equation (1.1). Under a proper re-scaler, the function at $z = z_1 \geq z_0$ can be approximated by

$$E(x,y,z_1) = 2p_1 e^{p_1\left(x^2+y^2\right)}, \quad (x,y) \in \mathcal{A}, \tag{2.1}$$

where $\mathcal{A}=\{(x,y):|x|,|y|\le r_0=2\sqrt{2}/q_1\}$, $p_1=1/[2(1+\mathbf{i}z_1)]$, $q_1=1/\sqrt{2\left(1+z_1^2\right)}$ [1,8]. Set $z_1=10^2$. In Figure 2.1, we show the field function E which is, by nature, highly oscillatory. This feature often makes a computational grid refinement extremely costly or even impossible.

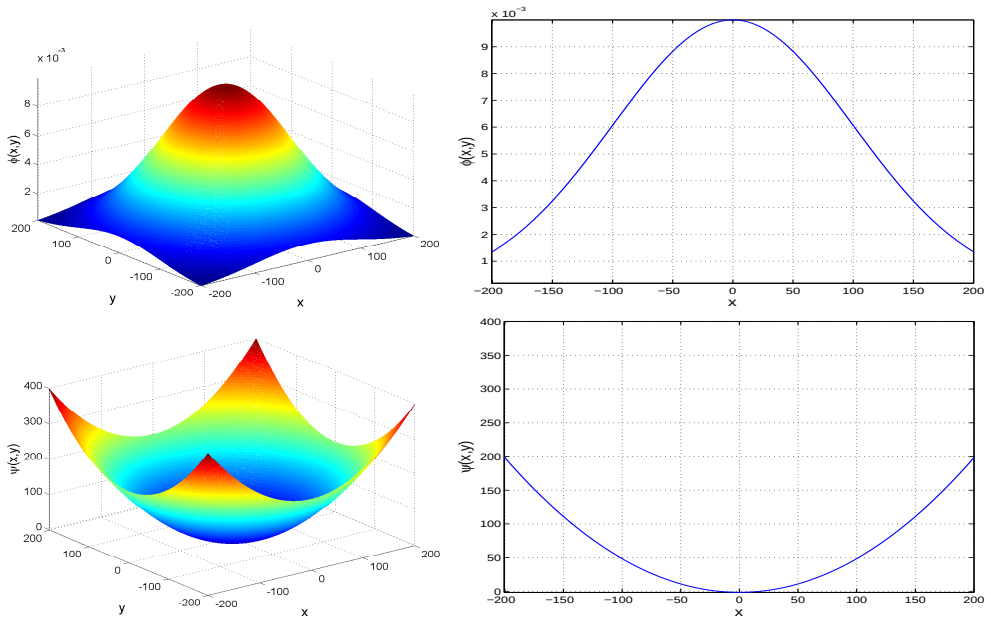

FIGURE 2.2. Functions ϕ and ψ corresponding to (2.1). Spatial steps $h_x=h_y=0.5$ are used. Again, the second column is for intersections with the Y-Z plane. The spacial domain is slightly reduced from its original size to match that in Figure 2.1.

Now, recall the mapping (1.3). It is not difficult to observe that (2.1) can be transformed into

$$E(x,y,z_1)=\phi(x,y,z_1)e^{\mathbf{i}\psi(x,y,z_1)},\quad (x,y)\in\mathcal{A},$$

where

$$\phi(x,y,z_1)=\sqrt{2}q_1e^{-q_1^2\left(x^2+y^2\right)}\text{ and }\psi(x,y,z_1)=q_1^2z_1\left(x^2+y^2\right)-\cos^{-1}q_1.$$

We simulate functions ϕ, ψ in Figure 2.2. Apparently, neither of them is oscillatory although the original complex field distribution E is highly oscillatory. The interesting observation indicates that relatively large step sizes can be employed if ϕ and ψ are the solutions to be sought. Needless to say, this implies a useful potential for the development of highly applicable, yet simple structured, numerical procedures to realize our ultimate goals in computational efficiency as well as accuracy. This encourages our continuing explorations in the eikonal splitting method via (1.3).

Let functions ϕ, ψ be sufficiently smooth and $\phi\neq0$. For the simplicity in notations, we denote $p=\kappa^2(\ell^2/\ell_0^2-1)$. Now, a substitution of (1.3) into (1.1) yields the following pair

of nonlinear differential equations,

$$\phi_z = \alpha\left(\psi_{xx}+\psi_{yy}\right)+f_1, \tag{2.2}$$
$$\psi_z = \beta\left(\phi_{xx}+\phi_{yy}\right)+f_2, \tag{2.3}$$

where

$$\alpha=\frac{\phi}{2},\ \beta=-\frac{1}{2\kappa^2\phi},\ f_1=\phi_x\psi_x+\phi_y\psi_y,\ f_2=\frac{1}{2}\left[(\psi_x)^2+(\psi_y)^2-p\right]. \tag{2.4}$$

Note that solutions of equations (2.2)–(2.4) are not oscillatory even when κ is large. As a consequence, mesh steps to be employed for the numerical solution can be relatively large. Needless to say, this makes fast computations of the paraxial differential equation (1.1) solution more realistic. In fact, elementary studies of different discretization procedures for (2.2)–(2.4) have been carried out in a number of recent publications (for instance, see [3,16,17] and references therein).

Although different finite difference approximations of (2.2) and (2.3) have been constructed, analysis of their numerical stabilities still need to be carefully explored. In fact, instabilities of certain eikonal schemes have been reported in laboratorial computations where particular large beam propagation distances are considered [7,16,18].

To comprise an ADI scheme, we may denote that

$$w=\begin{bmatrix}\phi\\ \psi\end{bmatrix},\ f=\begin{bmatrix}f_1\\ f_2\end{bmatrix},\ M=\begin{bmatrix}0 & \alpha\\ \beta & 0\end{bmatrix}. \tag{2.5}$$

Thus, (2.2) and (2.3) can be formulated in a matrix form,

$$w_z=Mw_{xx}+Mw_{yy}+f,\quad (x,y,z)\in\mathcal{D}. \tag{2.6}$$

In this paper, we consider a standard initial condition,

$$w(x,y,z_0)=g_0(x,y),\quad a\le x\le b,\ c\le y\le d, \tag{2.7}$$

where g_0 is sufficiently smooth, together with homogeneous Dirichlet boundary conditions,

$$\begin{aligned} &w(a,y,z)=w(b,y,z)=w(x,c,z)=w(x,d,z)=0,\\ &a\le x\le b,\ c\le y\le d,\ z\ge z_0. \end{aligned} \tag{2.8}$$

We note that applications of homogeneous Neumann, Robin, or transparent boundary conditions may lead to different amplification matrices in subsequent linear systems. But nevertheless, their discussions are similar. We will consider a second boundary condition in simulation experiments but leave detailed investigations to forthcoming papers.

Consider a three-dimensional mesh region $\mathcal{D}_{h,\tau}$ superimposing part of $\mathcal{D}$, where the spatial grids are uniform and grids in the light propagation direction are given by

$$z_\sigma=z_0+\sum_{k=0}^{\sigma-1}\tau_k,\ \sigma=0,1,2,\ldots.$$

Note that, while spatial steps $h_x=(b-a)/n$ and $h_y=(d-c)/n$ are fixed by a given integer n, τ_k are variable. Since the ADI scheme is of single step in z, without loss of generality, we use $\tau=\tau_k$ in our investigations although proper z-adaptations, such as the z-stretching strategy [7], can be introduced during any stages of computations.

We further adopt standard notations for the discretization of (2.5),

$$f^{\sigma}_{i,j}=(f_1(x_i,y_j,z_\sigma),f_2(x_i,y_j,z_\sigma))^{\mathsf{T}},\quad w^{\sigma}_{i,j}=(\phi(x_i,y_j,z_\sigma),\psi(x_i,y_j,z_\sigma))^{\mathsf{T}},$$

and, with (2.4),

$$M^{\sigma}_{i,j}=\begin{bmatrix} 0 & \alpha^{\sigma}_{i,j} \\ \beta^{\sigma}_{i,j} & 0 \end{bmatrix},\ \alpha^{\sigma}_{i,j}=\frac{\phi(x_i,y_j,z_\sigma)}{2},\ \beta^{\sigma}_{i,j}=-\frac{1}{2\kappa^2\phi(x_i,y_j,z_\sigma)}, \tag{2.9}$$

where

$$\kappa\gg 1,\ \max\phi\geq\phi(x_i,y_j,z_\sigma)\geq\min\phi>0,\quad (x_i,y_j,z_\sigma)\in\mathcal{D}_{h,\tau},$$

in which both $\min\phi$ and $\max\phi$ are independent of n [1,16].

Based on central finite differences in space, an ADI discretization of (2.6)–(2.8) yields the following coupled systems of equations,

$$(I_{2n^2}-\mu M^{\sigma})w^{\sigma+1/2} = (I_{2n^2}+\eta N^{\sigma})w^{\sigma}+\frac{\tau}{2}f^{\sigma}, \tag{2.10}$$

$$\left(I_{2n^2}-\eta N^{\sigma+1/2}\right)w^{\sigma+1} = \left(I_{2n^2}+\mu M^{\sigma+1/2}\right)w^{\sigma+1/2}+\frac{\tau}{2}f^{\sigma+1/2}, \tag{2.11}$$

$$(x_i,y_j,z_\sigma)\in\mathcal{D}_{h,\tau},$$

where I_k denotes a $k\times k$ identity matrix, $\mu=\tau/(2h_x^2)$ and $\eta=\tau/(2h_y^2)$ are dimensional Courant numbers, and for $i,j=1,2,\ldots,n$, $\sigma=0,1,2,\ldots$,

$$\begin{aligned} f^{\sigma} &= (f^{\sigma}_{1,1},f^{\sigma}_{2,1},\ldots,f^{\sigma}_{n,1},\ldots,f^{\sigma}_{n,n})^{\mathsf{T}}\in\mathbb{R}^{2n^2},\\ w^{\sigma} &= (w^{\sigma}_{1,1},w^{\sigma}_{2,1},\ldots,w^{\sigma}_{n,1},\ldots,w^{\sigma}_{n,n})^{\mathsf{T}}\in\mathbb{R}^{2n^2},\end{aligned}$$

$$M^{\sigma} = \operatorname{diag}(M^{\sigma}_1,M^{\sigma}_2,\ldots,M^{\sigma}_n) \tag{2.12}$$

with

$$M^{\sigma}_j = \begin{bmatrix} -2M^{\sigma}_{1,j} & M^{\sigma}_{1,j} & & \\ M^{\sigma}_{2,j} & -2M^{\sigma}_{2,j} & M^{\sigma}_{2,j} & \\ & \ddots & \ddots & \ddots \\ & & M^{\sigma}_{n,j} & -2M^{\sigma}_{n,j} \end{bmatrix},$$

and

$$N^{\sigma} = \begin{bmatrix} -2N^{\sigma}_1 & N^{\sigma}_1 & & \\ N^{\sigma}_2 & -2N^{\sigma}_2 & N^{\sigma}_2 & \\ & \ddots & \ddots & \ddots \\ & & N^{\sigma}_n & -2N^{\sigma}_n \end{bmatrix} \tag{2.13}$$

with

$$N_j^\sigma = \mathrm{diag}\left(M_{1,j}^\sigma, M_{2,j}^\sigma, \ldots, M_{n,j}^\sigma\right).$$

Given that $I_{2n^2} - \mu M^\sigma$ and $I_{2n^2} - \eta N^{\sigma+1/2}$ are invertible. Equations (2.10) and (2.11) can be conveniently converted to the following linear system

$$w^{\sigma+1/2} = (I_{2n^2} - \mu M^\sigma)^{-1}(I_{2n^2} + \eta N^\sigma) w^\sigma + \frac{\tau}{2} g_1^\sigma, \tag{2.14}$$

$$w^{\sigma+1} = \left(I_{2n^2} - \eta N^{\sigma+1/2}\right)^{-1}\left(I_{2n^2} + \mu M^{\sigma+1/2}\right) w^{\sigma+1/2} + \frac{\tau}{2} g_2^{\sigma+1/2}, \tag{2.15}$$

where

$$g_1^\sigma = (I_{2n^2} - \mu M^\sigma)^{-1} f^\sigma \quad \text{and} \quad g_2^{\sigma+1/2} = \left(I_{2n^2} - \eta N^{\sigma+1/2}\right)^{-1} f^{\sigma+1/2}.$$

Therefore

$$A_\sigma = (I_{2n^2} - \mu M^\sigma)^{-1}(I_{2n^2} + \eta N^\sigma), \tag{2.16}$$

$$P_\sigma = \left(I_{2n^2} - \eta N^{\sigma+1/2}\right)^{-1}\left(I_{2n^2} + \mu M^{\sigma+1/2}\right) \tag{2.17}$$

are amplification matrices corresponding to the eikonal ADI scheme implemented. Further, we denote

$$\begin{aligned} S^\sigma &= \mathrm{diag}(N_1^\sigma, N_2^\sigma, \ldots, N_n^\sigma) \in \mathbb{R}^{2n^2 \times 2n^2}, \\ L &= \mathrm{tridiag}(1, -2, 1) \in \mathbb{R}^{n \times n}, \\ T_1 &= I_n \otimes L \otimes I_2 \in \mathbb{R}^{2n^2 \times 2n^2}, \\ T_2 &= L \otimes I_{2n} \in \mathbb{R}^{2n^2 \times 2n^2}, \end{aligned}$$

where $\otimes$ stands for a standard Kronecker product [10]. We observe readily from (2.12) and (2.13) that

$$M^\sigma = S^\sigma T_1,\ N^\sigma = S^\sigma T_2.$$

3 Stability Analysis

It is apparently that the ADI method (2.14) and (2.15) is not stable in the classical von Neumann sense in general. This can be seen via a similar mesh structure investigated in [2]. However, on the other hand, the split scheme exhibits tremendous advantages in short distanced beam propagation simulations as compared with its peers [14, 16]. In fact, in highly oscillatory problem computations, excellent algorithmic simplicity and applicability are often more favorable [1, 6, 16]. Nevertheless, a straightforward asymptotic stability analysis can be extremely meaningful in applications.

Definition 3.1. Consider a finite difference method with an amplification matrix Φ for solving an oscillatory problem associated with a high wave number, that is, $\kappa \gg 1$. We say that the numerical method is asymptotically stable if there exists a constant $d > 0$ such that

$$\rho(\Phi) = 1 + O\left(\frac{1}{\kappa^d}\right),$$

where $\rho(\cdot)$ is the spectral radius and the constant d is called the asymptotical stability index of the method.

Since $d > 0$, we may notice that the higher the wave number is, the smaller the quantity $1/\kappa^d$ can be. In fact, $1/\kappa^d \to 0$ monotonically as $\kappa \to \infty$. As a consequence, the value of $\rho(\Phi)$ can be extremely close to the unity in most optical wave computations we have tested.

There are stronger, more rigorous and sophisticated stability criteria existing. Most of them, however, do not offer any direct assessment of contributions of the solution frequency to the numerical stability. This issue has become significant, or even crucial, when highly oscillatory wave functions are concerned [6,14,16]. Definition 3.1 provides a weaker, but simple and straightforward, tool for assessing algorithms for approximating solutions of highly oscillatory problems. It is proven to be effective in practical computations, and can be viewed as an extension of those for highly oscillatory integrals studied in [6].

Theorem 3.2. The oscillation-free eikonal transformation based ADI method (2.14), (2.15) is asymptotically stable with a stability index one.

We prove our result in following three steps.

STEP I. ESTIMATES OF MATRIX SPECTRAL RADII

Assume κ to be an arbitrary positive parameter. Let e_j be the jth column of the $2n^2 \times 2n^2$ identity matrix. Then

$$P = [e_1, e_3, \ldots, e_{2n^2-1}, e_2, e_4, \ldots, e_{2n^2}]$$

is a $2n^2 \times 2n^2$ permutation matrix. Furthermore, we have

$$P^\intercal S^\sigma P = \begin{bmatrix} 0 & \Lambda_\alpha^\sigma \\ \Lambda_\beta^\sigma & 0 \end{bmatrix},$$

where

$$\Lambda_\alpha^\sigma = \mathrm{diag}(\alpha_{1,1}^\sigma, \alpha_{2,1}^\sigma, \ldots, \alpha_{n,1}^\sigma, \alpha_{1,2}^\sigma, \ldots, \alpha_{n,n}^\sigma),$$
$$\Lambda_\beta^\sigma = \mathrm{diag}(\beta_{1,1}^\sigma, \beta_{2,1}^\sigma, \ldots, \beta_{n,1}^\sigma, \beta_{1,2}^\sigma, \ldots, \beta_{n,n}^\sigma),$$

in which $\alpha_{i,j}^\sigma$ and $\beta_{i,j}^\sigma$ are defined in (2.9). Moreover, we observe that

$$P^\intercal T_1 P = I_{2n} \otimes L \quad \text{and} \quad P^\intercal T_2 P = I_2 \otimes L \otimes I_n.$$

Thus,

$$P^\intercal M^\sigma P = P^\intercal S^\sigma T_1 P = \begin{bmatrix} 0 & \Lambda_\alpha^\sigma (I_n \otimes L) \\ \Lambda_\beta^\sigma (I_n \otimes L) & 0 \end{bmatrix} \equiv \widehat{M}_\sigma, \tag{3.1}$$

and

$$P^\intercal N^\sigma P = P^\intercal S^\sigma T_2 P = \begin{bmatrix} 0 & \Lambda_\alpha^\sigma (L \otimes I_n) \\ \Lambda_\beta^\sigma (L \otimes I_n) & 0 \end{bmatrix} \equiv \widehat{N}_\sigma. \tag{3.2}$$

Recall (2.9). Base on the definition of the spectral norm we have

$$\|\Lambda_\alpha^\sigma\|_2 = \frac{\max\phi}{2} = O(1), \qquad \|\Lambda_\beta^\sigma\|_2 = \frac{1}{2\kappa^2 \min\phi} = O\left(\frac{1}{\kappa^2}\right). \tag{3.3}$$

It follows immediately that $\|L\|_2 < 4 = O(1)$. This implies that

$$\|L \otimes I_n\|_2 = \|L\|_2 = O(1). \tag{3.4}$$

Consequently, we arrive at the following lemma.

Lemma 3.3. The spectra of M^σ and N^σ are bounded by $O(1/\kappa)$.

Proof. We first show that $\|\widehat{M}_\sigma^2\|_2 = O\left(1/\kappa^2\right)$. By (3.1), we have

$$\widehat{M}_\sigma^2 = \begin{bmatrix} \Lambda_\alpha^\sigma (L \otimes I_n) \Lambda_\beta^\sigma (L \otimes I_n) & 0 \\ 0 & \Lambda_\beta^\sigma (L \otimes I_n) \Lambda_\alpha^\sigma (L \otimes I_n) \end{bmatrix}.$$

Hence, according to (3.3) and (3.4),

$$\|\widehat{M}_\sigma^2\|_2 \le \|\Lambda_\alpha^\sigma\|_2 \|L \otimes I_n\|_2 \|\Lambda_\beta^\sigma\|_2 \|L \otimes I_n\|_2 = O\left(\frac{1}{\kappa^2}\right).$$

We thus conclude that

$$\rho(M^\sigma) = \rho(\widehat{M}_\sigma) = O\left(\frac{1}{\kappa}\right).$$

Analogously, by (3.2), we have

$$\|\widehat{N}_\sigma^2\|_2 = O\left(\frac{1}{\kappa^2}\right) \quad \text{and} \quad \rho(N^\sigma) = \rho(\widehat{N}_\sigma) = O\left(\frac{1}{\kappa}\right).$$

□

Although the above lemma provides strong estimates for matrices $\widehat{M}_\sigma^2$, $\widehat{N}_\sigma^2$, if we view κ as an arbitrary positive parameter, we still cannot claim that

$$\|\widehat{M}_\sigma\|_2,\ \|\widehat{N}_\sigma\|_2 = O\left(\frac{1}{\kappa}\right).$$

But nevertheless, we may show following useful results.

Lemma 3.4. The norms $\|\widehat{M}_\sigma\|_2$ and $\|\widehat{N}_\sigma\|_2$ are well bounded, i.e.,

$$\|\widehat{M}_\sigma\|_2,\ \|\widehat{N}_\sigma\|_2 = O(1).$$

Proof. According to (3.1), we have

$$\widehat{M}_\sigma \widehat{M}_\sigma^\intercal = (I_{2n} \otimes L) \begin{bmatrix} (\Lambda_\alpha^\sigma)^2 & 0 \\ 0 & (\Lambda_\beta^\sigma)^2 \end{bmatrix} (I_{2n} \otimes L).$$

Thus, by applying estimates (3.3) and (3.4), we obtain that

$$\|\widehat{M}_\sigma\|_2 = \sqrt{\rho(\widehat{M}_\sigma \widehat{M}_\sigma^\intercal)} \le \sqrt{4 \cdot \rho((\Lambda_\alpha^\sigma)^2) \cdot 4} = O(1).$$

The estimate $\|\widehat{N}_\sigma\|_2 = O(1)$ is analogously resulted. □

STEP II. A FINAL PREPARATION FOR THE ASYMPTOTICAL STABILITY

Recall (2.16). It is observed that

$$A_\sigma = (I_{2n^2} - \mu M^\sigma)^{-1} (I_{2n^2} + \eta N^\sigma) \equiv I_{2n^2} + B_\sigma,$$

where

$$B_\sigma = (I_{2n^2} - \mu M^\sigma)^{-1} (\eta N^\sigma + \mu M^\sigma).$$

In following discussions, we will complete a final preparation leading to

$$\left\|B_\sigma^2\right\|_2 = O\left(\frac{(\mu+\eta)^3}{\kappa^2}\right). \tag{3.5}$$

In conventional laser applications, values of κ range from 10^4 to 10^6. Therefore, without loss of generality, we may assume that both μ/κ and η/κ are much less than unity.

Similar to those in (3.1) and (3.2), we may permute B_σ by P in the following way:

$$\begin{aligned} \widehat{B}_\sigma &\equiv P^\intercal B_\sigma P \\ &= \left(I_{2n^2} - \mu \widehat{M}_\sigma\right)^{-1} (\eta \widehat{N}_\sigma + \mu \widehat{M}_\sigma) \\ &= \left(I_{2n^2} - \mu^2 \widehat{M}_\sigma^2\right)^{-1} \left(I_{2n^2} + \mu \widehat{M}_\sigma\right) (\eta \widehat{N}_\sigma + \mu \widehat{M}_\sigma) \\ &= \left(I_{2n^2} - \mu^2 \widehat{M}_\sigma^2\right)^{-1} \mu \widehat{M}_\sigma (\eta \widehat{N}_\sigma + \mu \widehat{M}_\sigma) + \left(I_{2n^2} - \mu^2 \widehat{M}_\sigma^2\right)^{-1} (\eta \widehat{N}_\sigma + \mu \widehat{M}_\sigma) \\ &\equiv C^{-1} M_1 + C^{-1} M_2, \end{aligned} \tag{3.6}$$

where

$$\begin{aligned} C &= I_{2n^2}-\mu^2\widehat{M}_\sigma^2 \\ &= \begin{bmatrix} I_{n^2}-\mu^2\Lambda_\alpha^\sigma(I_n\otimes L)\Lambda_\beta^\sigma(I_n\otimes L) & 0 \\ 0 & I_{n^2}-\mu^2\Lambda_\beta^\sigma(I_n\otimes L)\Lambda_\alpha^\sigma(I_n\otimes L) \end{bmatrix} \\ &\equiv \begin{bmatrix} C_1 & 0 \\ 0 & C_2 \end{bmatrix}, \qquad (3.7) \\ M_1 &= \mu\widehat{M}_\sigma(\eta\widehat{N}_\sigma+\mu\widehat{M}_\sigma), \qquad (3.8) \\ M_2 &= \eta\widehat{N}_\sigma+\mu\widehat{M}_\sigma=\begin{bmatrix} 0 & \Lambda_\alpha^\sigma L_2 \\ \Lambda_\beta^\sigma L_2 & 0 \end{bmatrix}, \qquad (3.9) \end{aligned}$$

in which $L_2=\mu I_n\otimes L+\eta L\otimes I_n$ and thus, consequently, $\|L_2\|_2=O(\mu+\eta)$.

The following lemma offers norm estimates for several most relevant matrices to be used in our final proof of the main theorem.

Lemma 3.5. Utilizing notations given in (3.6)–(3.9), we have

(i) $\|C^{-1}\|_2=O(1)$, and consequently $\|C_1^{-1}\|_2=O(1)$, $\|C_2^{-1}\|_2=O(1)$;

(ii) $\|C^{-1}M_1\|_2=O\left(\dfrac{\mu^2+\eta^2}{\kappa^2}\right)$;

(iii) $\|M_2\|_2=O(\mu+\eta)$;

(iv) $\|(C^{-1}M_2)^2\|_2=O\left(\dfrac{\mu^2+\eta^2}{\kappa^2}\right)$.

Proof. First, according to (3.7) and Lemma 3.3, we have

$$\|C\|_2\geq 1-\mu^2\|\widehat{M}_\sigma^2\|_2=1-O\left(\mu^2/\kappa^2\right).$$

Note the fact that the ratio μ/κ is sufficiently small. We thus conclude that $\|C^{-1}\|_2=O(1)$. On the other hand, from (3.7), it can be observed that $\|C_1^{-1}\|_2=O(1)$ and $\|C_2^{-1}\|_2=O(1)$ by definitions of the matrices. This completes our proof of (i).

Further, by (3.8), we have

$$M_1=\mu\eta\widehat{M}_\sigma\widehat{N}_\sigma+\mu^2\widehat{M}_\sigma^2.$$

Recall Lemma 3.3. The second term on the right-hand side of the above equation obeys the estimate $\|\mu^2\widehat{M}_\sigma^2\|_2=O(\mu^2/\kappa^2)$.

Now, we can observe from (3.1) and (3.2) that

$$\widehat{M}_\sigma\widehat{N}_\sigma=\begin{bmatrix} \Lambda_\alpha^\sigma(L\otimes I_n)\Lambda_\beta^\sigma(I_n\otimes L) & 0 \\ 0 & \Lambda_\beta^\sigma(L\otimes I_n)\Lambda_\alpha^\sigma(I_n\otimes L) \end{bmatrix}.$$

Therefore, according to (3.3),

$$\|\widehat{M}_\sigma \widehat{N}_\sigma\|_2 = O\left(1/\kappa^2\right).$$

It follows further that $\|C^{-1}M_1\|_2 = O\left(\dfrac{\mu^2+\eta^2}{\kappa^2}\right)$ and this ensures (ii).

As for (iii), based on (3.9), we find that

$$\|M_2\|_2 = \sqrt{\rho(M_2 M_2^{\mathsf{T}})} = \sqrt{\rho(L_2(\Lambda_\alpha^\sigma)^2 L_2)} = O(\mu+\eta).$$

On the other hand, a straightforward matrix multiplication leads to

$$C^{-1}M_2 = \begin{bmatrix} 0 & C_2^{-1}\Lambda_\alpha L_2 \\ C_1^{-1}\Lambda_\beta L_2 & 0 \end{bmatrix}.$$

This indicates that

$$\left(C^{-1}M_2\right)^2 = \begin{bmatrix} C_2^{-1}\Lambda_\alpha L_2 C_1^{-1}\Lambda_\beta L_2 & 0 \\ 0 & C_1^{-1}\Lambda_\beta L_2 C_2^{-1}\Lambda_\alpha L_2 \end{bmatrix}.$$

Note that $\|C_1^{-1}\|_2, \|C_2^{-1}\|_2 = O(1)$, $\|\Lambda_\alpha\|_2 = O(1)$, $\|L_2\|_2 = O(\mu+\eta)$ and $\|\Lambda_\beta\|_2 = O(1/\kappa^2)$ from our existing results. Consequently,

$$\|(C^{-1}M_2)^2\|_2 \le \|C_2^{-1}\|_2\|\Lambda_\alpha\|_2\|L_2\|_2\|C_1^{-1}\|_2\|\Lambda_\beta\|_2\|L_2\|_2 = O\left(\frac{\mu^2+\eta^2}{\kappa^2}\right).$$

This completes our proof. □

STEP III. ESTIMATES OF THE AMPLIFICATION MATRICES

We first show that

$$\|\widehat{B}_\sigma^2\|_2 = O\left((\mu+\eta)^3/\kappa^2\right).$$

Recall (3.6). By using Lemma 3.5 we acquire that

$$\begin{aligned}
\|\widehat{B}_\sigma^2\|_2 &= \|(C^{-1}M_1)^2 + (C^{-1}M_2)^2 + C^{-1}M_1C^{-1}M_2 + C^{-1}M_2C^{-1}M_1\|_2 \\
&\le \|(C^{-1}M_1)^2\|_2 + \|(C^{-1}M_2)\|_2^2 + \|C^{-1}\|_2\|M_1\|_2\|C^{-1}\|_2\|M_2\|_2 \\
&\quad + \|C^{-1}\|_2\|M_2\|_2\|C^{-1}\|_2\|M_1\|_2 \\
&= O\left(\frac{\mu^2+\eta^2}{\kappa^2}\right) + O\left(\frac{\mu^4+\eta^4}{\kappa^4}\right) + O\left(\frac{\mu^3+\eta^3}{\kappa^2}\right) + O\left(\frac{\mu^3+\eta^3}{\kappa^2}\right) \\
&= O\left(\frac{\mu^3+\eta^3}{\kappa^2}\right).
\end{aligned}$$

The above result ensures the following estimate,

$$\rho(A_\sigma) = 1 + \rho(B_\sigma) = 1 + O\left(\frac{(\mu+\eta)^{3/2}}{\kappa}\right).$$

Now, recall (2.17). By the same token, we may show analogously that

$$\rho(P_\sigma)=1+O\left(\frac{(\mu+\eta)^{3/2}}{\kappa}\right).$$

Therefore Theorem 3.2 must be true. This indicates that if the Courant numbers η and μ are bounded, then the eikonal transformation based ADI finite difference scheme (2.14), (2.15) is asymptotically stable with an asymptotical stability index one. This completes our arguments.

4 Numerical Experiments and Concluding Remarks

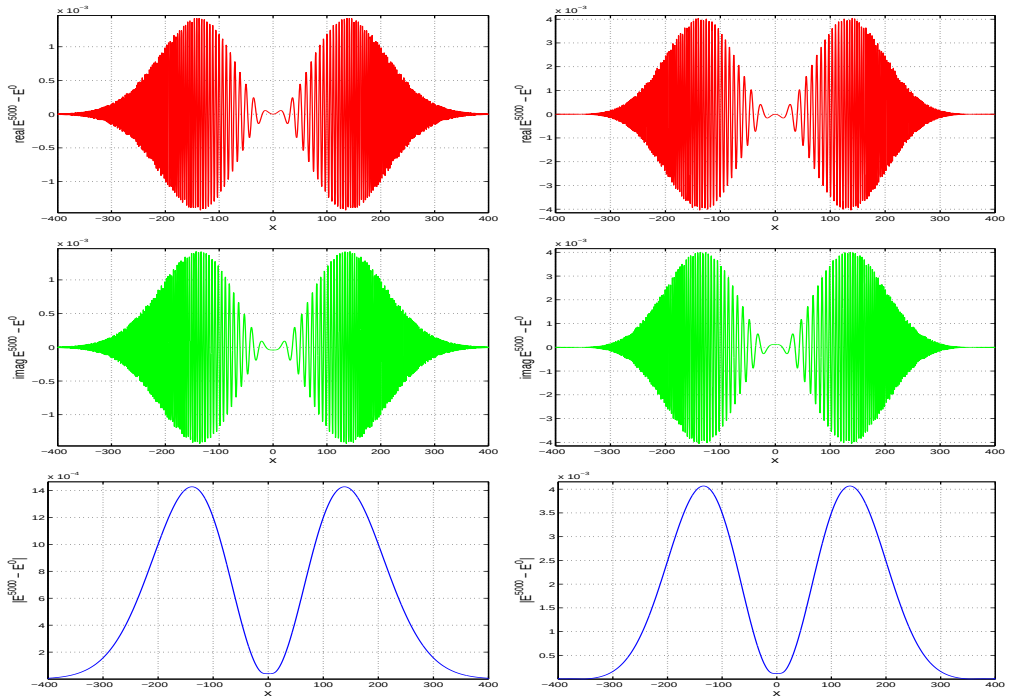

FIGURE 4.1. Y-Z intersections of the real part, imaginary part, and modulus of the difference between the recovered highly oscillatory solution E^{5K} and the initial function E^0 (from the top to bottom; LEFT: $p=0$, RIGHT: $p=100$.). $\tau=0.32$ is used.

Purpose of this section is to demonstrate the structure simplicity and numerical stability of the eikonal transformation based ADI method through self-contained tests and experiments. To this end, we let $p(x,y,z)\equiv p$ be a constant. Based on (1.1) we consider the following typical paraxial model along with homogeneous boundary conditions [16],

$$2\mathbf{i}\kappa E_z = E_{xx}+E_{yy}-p\kappa^2 E,\quad (x,y)\in\mathcal{A},\ z>z_1, \tag{4.1}$$

$$E_\gamma = 0,\quad (x,y)\in\partial\mathcal{A},\ z\geq z_1, \tag{4.2}$$

$$E(x,y,z_1) = 2p_1 e^{p_1\left(x^2+y^2\right)},\quad (x,y)\in\mathcal{A}, \tag{4.3}$$

where $\partial\mathcal{A}$ is the boundary of $\mathcal{A}$, E_γ is the normal derivative of E along $\partial\mathcal{A}$ and $\mathcal{A}$, p_1, q_1 are defined in (2.1). The problem (4.1)–(4.3) facilitated by a constant p has been playing an extremely important role in monochromatic laser beam modeling and propagation computations. A reliable numerical solver must possess a long term stability until the traveling beam focuses or collapses for target oriented applications [8, 9, 17]. Therefore, differences between numerical solutions over large amounts of z-advancements are traditionally used as an important examination. This is also adopted in following experiments. Two different values of p, namely, $p=0$ and $p=100$, are considered.

Without loss of generality, we take $\kappa=10^4$, $z_1=100$ together with sufficiently large spacial step sizes $h_x=h_y=0.4$. We further adopt dimensional Courant numbers $\mu=\eta=5.0$, 2.0, which lead to transverse step sizes $\tau_1=0.8, \tau_2=0.32$, respectively, for the implicit numerical method. Central difference approximations are adopted for approximating the derivative functions involved in f_1 and f_2, that is,

$$(\phi_x)^\sigma_{i,j}\approx\frac{\phi^\sigma_{i+1,j}-\phi^\sigma_{i-1,j}}{2h_x},\qquad (\phi_y)^\sigma_{i,j}\approx\frac{\phi^\sigma_{i,j+1}-\phi^\sigma_{i,j-1}}{2h_y};$$
$$(\psi_x)^\sigma_{i,j}\approx\frac{\psi^\sigma_{i+1,j}-\psi^\sigma_{i-1,j}}{2h_x},\qquad (\psi_y)^\sigma_{i,j}\approx\frac{\psi^\sigma_{i,j+1}-\psi^\sigma_{i,j-1}}{2h_y}$$
$$i,j=1,2,\ldots,n\ \sigma=1/2,1,3/2,\ldots$$

On the Matlab platform, we first advance for 5000 steps in the transverse direction with τ_1. Then the experiment is repeated with τ_2 for 12500 steps in the z-direction. Numerical solutions acquired from two tests agree precisely at terminal location $z=4000$ and absolute errors between them are neglectful. As an illustration of the stable evolution of the numerical solutions, in Figure 4.1, we show differences of the real part, imaginary part, and modulus of the numerical solution at $z=4000$ as compared with that of the initial function (4.3). The computed energy functions of the laser wave indicate an excellent consistency with their expected physical features, although we may find that amplitudes of the function E become significantly large in the $p=100$ case as compared with the $p=0$ case. This phenomenon is physically correct.

Now, to exam further the numerical stability in an extreme fashion, together with $h_z=0.8$ and $\mu=\eta=5.0$, we advance underlying ADI calculations up to $z=8000$ in 10000 steps. The decomposed real and imaginary parts of the numerical solution E^{8000} is given in Figure 4.2. A three-dimensional modulus plot of the field function is presented in Figure 4.3. It is interesting that both sets of solutions exhibit the correct wave patterns precisely. This is especially important to the design of beam propagations in nano or micro devices [13, 14].

We further plot the difference between modulus of the computed solution $E(x,y,z_{8000})$ and $E(x,y,z_1)$, where $z_{8000}=z_1+8000\tau$, in Figure 4.4 for $p=0,100$, respectively. We may notice a significant difference between the case with nontrivial source term and without a source tern. However, both differences follow precisely the pattern of the modulus functions and stay as limited as compared with their respective electric fields E.

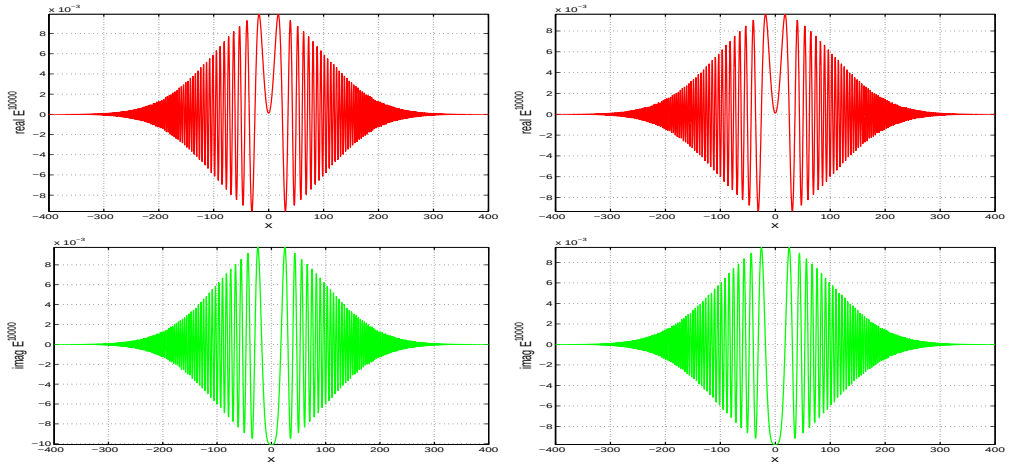

FIGURE 4.2. Y-Z intersections of the real and imaginary parts of the recovered highly oscillatory wave solution E^{10K} in 10000 z-steps (from the top to bottom; LEFT: $p=0$, RIGHT: $p=100$.).

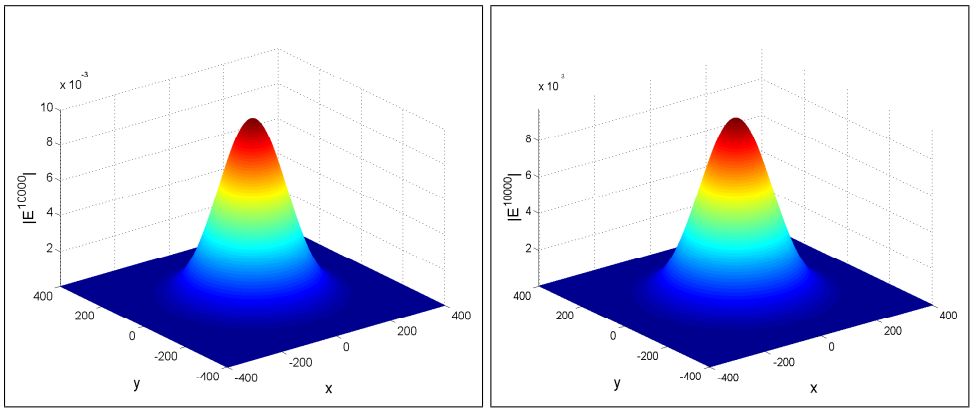

FIGURE 4.3. A three-dimensional view of the modulus of the field distribution E^{10K}. 10000 z-steps are executed with $h_x=h_y=0.4$, $\tau=0.8$ (LEFT: $p=0$, RIGHT: $p=100$.).

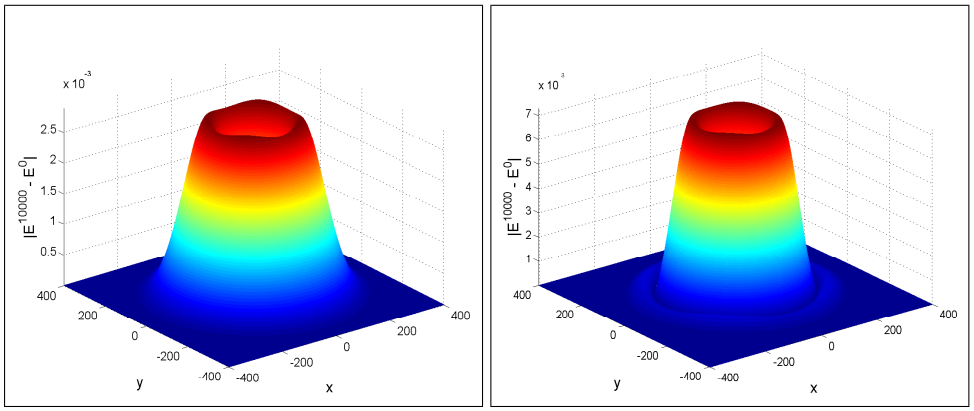

FIGURE 4.4. A three-dimensional view of the difference in modulus between the numerical solution E^{10K} and initial function E^0. Solutions are advanced up to 10000 z-steps with $h_x=hy=0.4$, $\tau=0.8$ (LEFT: $p=0$, RIGHT: $p=100$.)

To summarize, in this paper, via rigorous matrix spectrum analysis, we have proved the asymptotical stability of the ray transformation based finite difference method (2.14) and (2.15), which arises in the development of fast and accurate numerical methods for solving the paraxial wave equation (1.1). This result ensures the applicability and basic reliability of the splitting computations for highly oscillatory problems, in particular in near focusing optical computations. Similar analysis can be fulfilled for the local one-dimensional (LOD) method [15,16,18]. The novel eikonal splitting is not only simple and straightforward, but also oscillation-free in computations. Thus relatively large steps can be utilized, as demonstrated in our numerical examples. Further, the eikonal scheme is capable of solving problems with linear source terms. In the event if a nonlinear source term is preferred in equation (1.1) or (4.1), a proper linearization should be employed prior to an application of the eikonal splitting procedure.

The matrix investigation conducted in this paper can also be extended for examining similar oscillation-free algorithms, in particular eikonal transformation based methods for solving different Gaussian beam oriented problems such as Kukhtarev systems in photorefractive wave and wave-material interaction computations [1,13,18], and Maxwell's equations in large electromagnetic fields [5, 6]. Although asymptotic discussions involving (2.14) and (2.15) currently exist only with homogeneous first and second boundary conditions and uniform spacial grids, transparent or nonlocal boundary conditions together with grid adaptations [15, 16] may also be applied. In addition, more advanced splitting strategies, such as the adaptive splitting, iterative splitting, and asymptotic splitting [2, 15, 16, 18], can also be incorporated with the eikonal transformation. The study of eikonal formulas accommodating multi-valued ϕ, ψ functions, more rigorous stability definitions associated with highly oscillatory wave applications, however, are still in its infancy. These are, needless to say, among our future endeavors.

Acknowledgments

The authors would like to thank the referees for their breadth of knowledge and valuable suggestions which helped to improve the content and presentation of this paper. The study of the first author was supported in part by a URC Award from the Baylor University. The second author appreciates very much the University of Macau for the research grant (No. MYRG140(Y1-L2)-FST11-SHW) which enabled this collaborative study.

References

[1] Y. B. Band, Light and Matter: Electromagnetism, Optics, Spectroscopy and Lasers, John Wiley & Sons, West Sussex, 2006.

[2] M. A. Beauregard and Q. Sheng, An adaptive splitting approach for the quenching solution of reaction-diffusion equations over nonuniform grids, reprint, 2011.

[3] M. O. Bristeau, J. Erhel, P. Féat, R. Glowinski and J. Periaux, Solving the Helmholtz equation at high-wave numbers on a parallel computer with a shared virtual memory, Int. High Perfor. Comput. Appl., 9 (1995), 18–28.
[4] V. R. Chinni, C. R. Menyuk, and P. K. Wai, Accurate solution of the paraxial wave equation using Richard extrapolation, IEEE Photonics Tech. Lett., 6 (1994), 409–411.
[5] M. Condon, A. Deaño and A. Iserles, On highly oscillatory problems arising in electronic engineering, Math. Model. Numer. Anal., 43 (2009), 785–804.
[6] B. Engquist, A. Fokas, E. Hairer and A. Iserles, Highly Oscillatory Problems, London Math. Soc., London, 2009.
[7] L. Gonzalez, S. Guha, J. W. Rogers and Q. Sheng, An effective z-stretching method for paraxial light beam propagation simulations, J. Comput. Phys., 227 (2008), 7264–7278.
[8] J. W. Goodman, Introduction to Fourier Optics, Third Edition, Roberts & Company Publishers, Denver, 2004.
[9] S. Guha, Validity of the paraxial approximation in the focal region of a small-f-number lens, Optical Lett., 26 (2001), 1598–1600.
[10] R. Horn and C. Johnson, Topics in Matrix Analysis, Cambridge University Press, Cambridge, 1991.
[11] S. Jin, H. Wu, X. Yang and Z. Huang, Bloch decomposition-based Gaussian beam method for the Schrödinger equation with periodic potentials, J. Comput. Phys., 229 (2009), 4869–4883.
[12] M. F. Levy, Perfectly matched layer truncation for parabolic wave equation models, Proc. Royal Soc. Lond., 457 (2001), 2609–2624.
[13] B. E. A. Saleh and M. C. Teich, Fundamentals of Photonics, John Wiley & Sons, New York, 1991.
[14] M. A. Saleh, P. P. Banerjee, J. Carns, G. Cook and D. R. Evans, Stimulated photorefractive backscatter leading to six-wave mixing and phase conjugation in iron-doped lithium niobate, Appl. Optics, 46 (2007), 6151–6160.
[15] Q. Sheng, Adaptive decomposition finite difference methods for solving singular problems-a review, Front. Math. China, 4 (2009), 599–626.
[16] Q. Sheng, S. Guha and L. Gonzalez, An exponential transformation based splitting method for fast computations of highly oscillatory solutions, J. Comput. Appl. Math., 235 (2011), 4452–4463.
[17] N. P. van der Aa, The Rigorous Coupled-Wave Analysis, Ph.D. dissertation, Faculteit Wiskunde & Informatica, Technische Universiteit Eindhoven, the Netherland, 2007.
[18] W. P. Zang, J. G. Tian, Z. B. Liu, W. Y. Zhou, F. Song and C. P. Zhang, Local one-dimensional approximation for fast simulation of Z-scan measurements with an arbitrary beam, Appl. Optics, 43 (2004), 4408–4414.